Article

Structures of the nematic and cholesteric layers with tangential-conical boundary conditions

Mikhail N. Krakhalev [1,2]*, Rashid G. Bikbaev [1,2], Vitaly S. Sutormin [1], Ivan V. Timofeev [1,2] and Victor Ya. Zyryanov [1]

[1] Kirensky Institute of Physics, Federal Research Center KSC SB RAS, Krasnoyarsk 660036, Russia; bikbaev@iph.krasn.ru (R.G.B.); sutormin@iph.krasn.ru (V.S.S.); tiv@iph.krasn.ru (I.V.T.); zyr@iph.krasn.ru (V.Y.Z.)
[2] Siberian Federal University, Krasnoyarsk 660041, Russia
* Correspondence: kmn@iph.krasn.ru; Tel.: +7-391-249-4510

Version March 27, 2019 submitted to Crystals

Abstract: Orientational structures formed in nematic and cholesteric layers with tangential-conical boundary conditions are investigated. LC cells with one substrate specifying the conical surface anchoring and another substrate specifying the tangential one were considered. Director configurations and topological defects have been identified analyzing the texture patterns obtained by polarizing microscope in comparison with the structures and optical textures calculated by free energy minimization procedure of director eld and finite-difference time-domain method, respectively. The domains, periodic structures and two-dimensional defects, which are specific only for LC cells with tangential-conical anchoring, are studied depending on the layer thickness and cholesteric pitch.

Keywords: liquid crystal; cholesteric; nematic; conical boundary conditions; orientational structure; director configuration; topological defect

1. Introduction

Cholesteric liquid crystals (CLCs) are characterized by the helicoidal structure of director **n** (the unit vector indicating the preferred orientation of the long axes of liquid crystal (LC) molecules). These media have unique structural and optical properties [1]. CLCs can be used in various applications such as electro-optical devices with memory effect [2,3], quantum generation of light [4,5], switchable diffraction gratings [6–10], optical rotators [11], formation of colloidal systems with periodic distribution of particles [12], etc. The applications require various stable and metastable orientational structures depending on the boundary conditions, LC material parameters, ratio between LC layer thickness d and cholesteric pitch p, external factors [1,13–15]. For example, the homeotropic director configuration is formed in the cells at normal CLC anchoring with substrates and confinement ratio $d/p < K_{33}/2K_{22}$, where K_{22}, K_{33} are the twist and bend elastic constants, respectively [16–18]. The electric field applied to such cells causes the formation of bubble or elongated domains if the cholesteric pitch is slightly larger than the thickness of LC layer [19,20]. Besides, the topological soliton-like structures can be obtained using laser radiation [21,22] or the thermal quenching process [23]. At tangential anchoring of CLC with substrates, the Grandjean planar texture or domain structures are formed [3,13,24,25]. The structure with a periodic director modulation can be obtained in LC cells with certain confinement ratios d/p by application of electric field [7,26]. Under hybrid surface anchoring in the cell (one substrate specifies the tangential boundary conditions and another substrate specifies the normal ones) with confinement ratio $d/p > 1$, the structure of modulated hybrid-aligned cholesteric is formed, which can be controlled by light [9], temperature [10] or electric field [27].

The structures of cholesteric with conical boundary conditions have not been well studied yet. Smooth transformations of cholesteric orientational structures induced by the modification of normal surface anchoring to tangential one through formation of tilted or conical boundary conditions have been observed in [28,29]. Modulated structure of cholesteric under tangential surface anchoring at one of substrates and weak conical boundary conditions at the opposite side, which are formed at the interface of CLC and its isotropic phase, have been investigated in [30]. It has been shown that the period of director modulation is equal to the cholesteric pitch and orientation of periodic structure depends linearly on the confinement ratio d/p. At that, the critical d/p value for formation of modulated structure depends on the ratio of elastic constants, and for some CLCs it was less than in the case of normal or hybrid surface anchoring.

In present work the nematic and cholesteric structures formed in the LC cells with tangential-conical boundary conditions have been investigated.

2. Materials and Methods

2.1. Experimental

The experiment was carried out with sandwich-like cells consisting of two glass substrates coated with polymer films and the LC layer between them. Bottom substrate was covered by the polyvinyl alcohol (PVA) (Sigma Aldrich) and the top one was covered by the poly(isobutyl methacrylate) (PiBMA) (Sigma Aldrich). The polymer films were deposited on the substrates by spin coating. The PVA film was unidirectionally rubbed while the PiBMA film was not treated after the deposition process. The LC layer thickness d assigned by the glass microspheres was measured by means of the interference method with spectrometer HR4000 (Ocean Optics) before the filling process. The nematic mixture LN-396 (Belarusian State Technological University) and LN-396 doped with the left-handed chiral additive cholesterylacetate (Sigma Aldrich) were used as nematic and cholesteric, respectively. The helical twisting power HTP = $6.9\,\mu\text{m}^{-1}$ of cholesterylacetate in the LN-396 was determined using the Grandjean-Cano method. The cholesteric pitch p of used mixtures was calculated from $p = 1/(HTP \times c_w)$, where c_w is weight concentration of the chiral additive. The LC cells with the confinement ratios d/p of 0.14, 0.28, 0.43, 0.60, 0.78 and 0.88 were investigated by means of the polarizing optical microscope (POM) Axio Imager.A1m (Carl Zeiss).

2.2. Computer simulations

The nematic orientational structure inside the domain was calculated using the free energy minimization procedure of director field described in detail in ref. [31]. The domain wall orientational structure was analytically interpolated between the neighbouring domain structures. The values of $\theta(x)$ and/or $\varphi(x)$ were asymptotically reversed approaching the domain bulk value with multiplication by $\tan^{-1}(4x/L)\cdot 2/\pi$, where L is a characteristic wall thickness.

The optical properties of LC structures were calculated by Finite-Difference Time-Domain (FDTD) method. LC structure was illuminated from below by the plane wave with normal incidence along z-axis and polarization perpendicular to the rubbing direction. The plane wave source was located at the bottom boundary of the LC layer. Periodic boundary conditions were applied at the lateral boundaries of the simulation box (along the x and y axes), while the perfectly matched layers (PML) were used on the remaining top and bottom sides. The components of the electric field were calculated at the top boundary of the LC layer. POM images were obtained for the wavelength of incident light $\lambda = 602\,\text{nm}$.

3. Results and Discussion

3.1. Nematic layer

PVA film orients the nematic LN-396 tangentially while PiBMA film specifies the conical boundary conditions with the tilt angle of director θ_d = 50° [32–34] and azimuthal degeneration. The azimuthal degeneration is eliminated by presence of rubbed PVA film on the bottom substrate specifying the director orientation with azimuthal angle φ_0 = 0°. As a result, the orientational structure with zero azimuthal angle of director is formed in the cells including the LC-PiBMA interface (Fig. 1). At that, two types of domains differing by the tilt angles $+\theta_d$ and $-\theta_d$ on the PiBMA film are observed. The similar situation was in the LC cell with tangential-conical boundary conditions in the case of formation of conical surface anchoring at the interface of LC-isotropic phase [35]. Domains are separated from each other by defect walls which are clearly observed on the optical textures using polarized light when the polarization of incident light coincides with rubbing direction of PVA film. In the case of orthogonal orientation of polarizer and rubbing direction of PVA film these defect walls are almost invisible (see Suppl. Fig.S1). When the LC cell is placed between crossed polarizers the segments of wall with orientation differing from rubbing direction are clearly observed (Fig. 1a) indicating the presence of twist deformation of the director. The similar situation was observed in the domain walls formed by the application of the magnetic field [36].

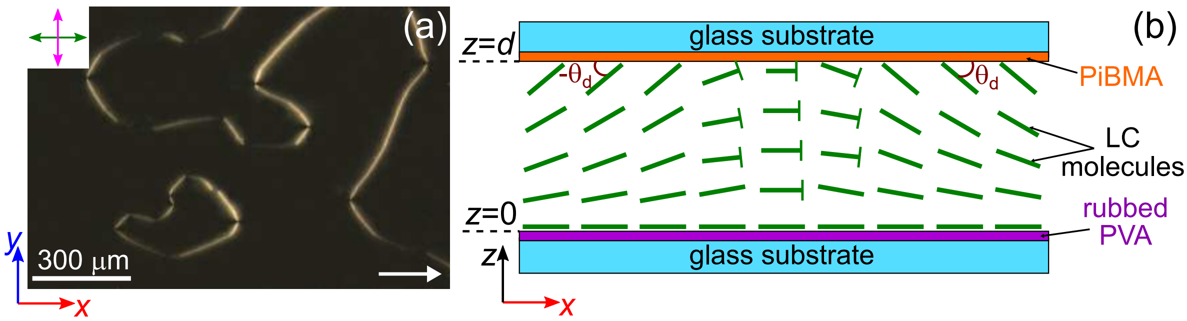

Figure 1. POM photo of LN-396 nematic layer with PiBMA film on the top substrate ($z = d$) and rubbed PVA film on the bottom one ($z = 0$) (a). The scheme of LC orientation in domains with tilt angle of director $+\theta_d$ and $-\theta_d$ on the PiBMA film (b). The LC layer thickness is $d = 21\ \mu$m. Hereinafter, the polarizer and analyzer directions are indicated by the magenta and green double arrows, respectively. The single arrow is the rubbing direction of PVA film.

The azimuthal angle of director rotation φ_d on the top substrate covered with PiBMA film can be measured by means of the analyzer rotation (Fig. 2). If the polarization of incident light is orthogonal to the director on the entrance substrate covered with PVA film and Mauguin condition is valid then the darkest areas of optical texture for twisted director configuration correspond to the parallel orientation of analyzer and director projection on the plane of output substrate covered with PiBMA film. Thus, the topology of director projection by the area of substrate covered with PiBMA can be determined.

The optical textures of nematic layer for different β angles between analyzer and rubbing direction of PVA film (Fig. 2a-h) and the director orientation on the PiBMA film near the domain wall (Fig. 2i) are presented in Fig. 2. The analysis by the above-mentioned technique revealed that there is the smooth azimuthal rotation of director from $\varphi_d = 0$ (far away from the wall) to the value φ_d in the center of the wall where the director is parallel to its plane. This rotation occurs at the distance of approximately the LC layer thickness. The domain wall contains the reversing points [37], dividing the segments of the wall with different director orientation relative to rubbing direction. The direction of azimuthal rotation (the φ sign) is defined by the condition that the absolute value of azimuthal angle of rotation on the substrate covered with PiBMA does not exceed $\pi/2$ value.

The cross-section of the domain wall is shown in Fig. 3a. The angle between the wall plane and rubbing direction is 60°. The orientational structure was calculated by the minimization of elastic

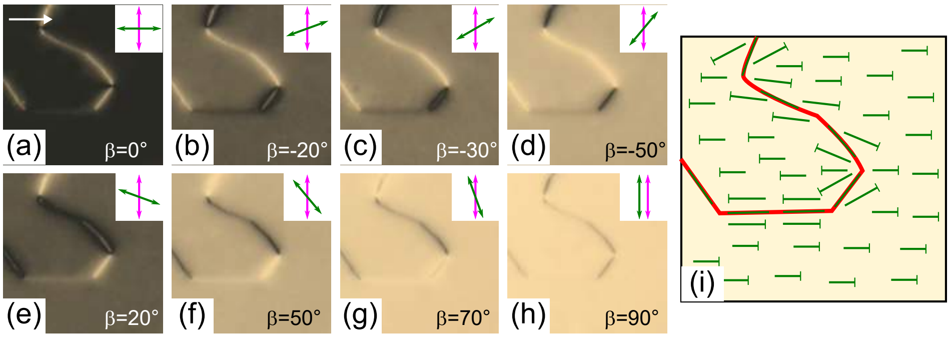

Figure 2. POM photos of sample area presented in Fig. 1. The polarizer is perpendicular to the rubbing direction of PVA film. The β angle between the analyzer and rubbing direction is 0° (a), -20° (b), -30° (c), -50° (d), 20° (e), 50° (f), 70° (g), 90° (h). Corresponding scheme of director orientation at the top substrate covered with PiBMA (i). The domain wall is indicated by the red line.

energy and analytical interpolation of director between two neighboring domains. The POM photos of domain wall segment for the different β angles have been obtained by the FDTD method based on the calculated orientational structure (Fig. 3b). When the analyzer is parallel to the rubbing direction ($\beta = 0°$) the darkest area is observed far away from the wall. At the same time, the center of domain wall is bright. The variation of β angle leads to the appearance of a couple of dark areas (extinction bands) merging at the center line of the wall at $\beta = -60°$ corresponded to the parallel orientation of the analyzer and the wall. The director orientation near the domain wall on the substrate with conical boundary conditions ($z = d$) is shown in Fig. 3c. The calculated data are in a good agreement with experiment.

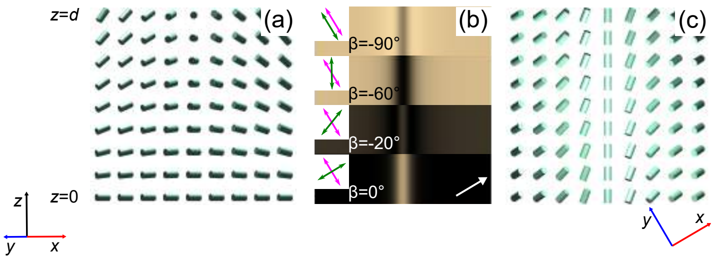

Figure 3. The calculated director configuration of nematic near the domain wall (a). The image of segment of domain wall for different β angles between analyzer and rubbing direction obtained by the FDTD method (b). The director orientation near the domain wall on the substrate covered with PiBMA film (c).

3.2. *Twisted cholesteric structure*

In the general case, the Mauguin condition is not valid for the homogeneously twisted structure of LC. However, the layer thickness of LC and wavelength of incident light can be chosen so that the Gooch-Terry minimum condition is valid for linearly polarized light passed through the LC cell [38]. This condition is independent of the rotation angle of director [39]. The twisted structure with azimuthal angle of director rotation depended on confinement ratio d/p is formed in the cholesteric cell with tangential-conical boundary conditions (Fig. 4a). The tilt and azimuthal angles of the director in the cholesteric bulk were calculated by the minimization of elastic energy for three d/p ($d = 6.5\,\mu$m) values (Fig. 4a). The ellipticity angle ε for polarized light with wavelength $\lambda = 602$ nm was determined based on these data (Fig. 4b). One can see that Gooch-Terry minimum condition is nearly independent of confinement ratio d/p as in the case of the homogeneously twisted LC structure. Used LC layer thickness and wavelength of incident light nearly correspond to Gooch-Terry minimum condition and the ε value do not exceed 5° after passing the linearly polarized light through the cell with $d/p = 0.14$, $d/p = 0.28$, $d/p = 0.44$. Thus, the method of analyzer rotation can be used for measuring of azimuthal angle φ_d of director on the top substrate covered with PiBMA. POM photos of samples with LC layer thickness $d = 6.5\,\mu$m and confinement ratio $d/p = 0.14$, $d/p = 0.28$ are shown in Fig. 4c-f. One can see that the monodomains corresponding to the opposite values of tilt angle θ_d in the cell with confinement ratio $d/p = 0.14$ have the larger size (Fig. 4c,d) than in the nematic LC cells (Fig. 1). The darkest state of domains is observed for $\beta = 37°$ when the interference filter ($\lambda = 602$ nm) is used (Fig. 4d). Thus, the azimuthal angle of director rotation at the substrate covered with PiBMA is $\varphi_d \cong 37°$. The monodomain structure is formed in the cell with confinement ratio $d/p = 0.28$ (Fig. 4e,f). The darkest state of domain (for incident light with wavelength $\lambda = 602$ nm) is observed for $\beta = 75°$ and, consequently, $\varphi_d \cong 75°$. Thus, the experimentally measured φ_d values are in a good agreement with theoretical calculation.

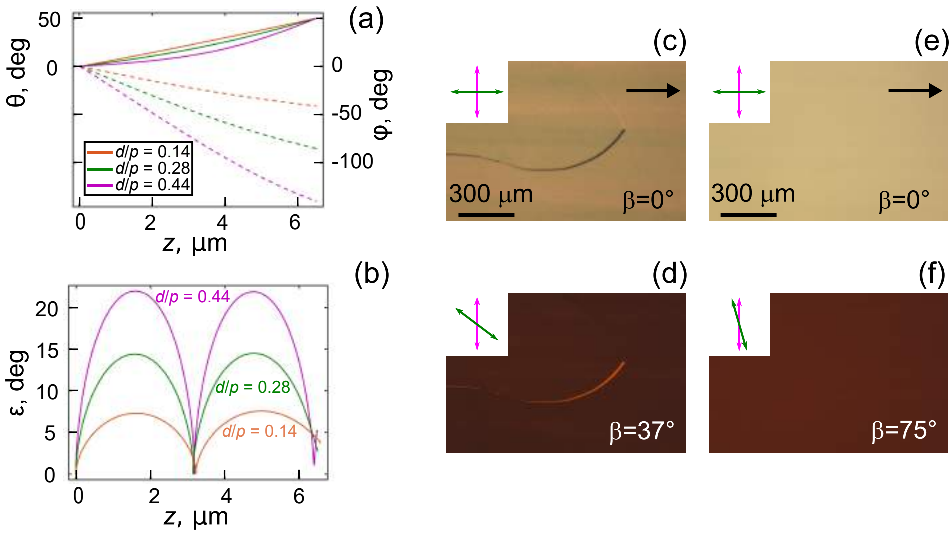

Figure 4. Calculated dependences of tilt angle $\theta(z)$, azimuthal angle $\varphi(z)$ (a) and corresponding dependence of ellipticity angle $\varepsilon(z)$ (b) for samples with $d/p = 0.14$ (orange line), $d/p = 0.28$ (green line) and $d/p = 0.44$ (magenta line). POM photos of cholesteric layer with confinement ratio $d/p = 0.14$ (c), (d) and $d/p = 0.28$ (e), (f). Photos are taken using white light when β angle between analyzer and rubbing direction of PVA film is 0° (c) and (e). Photos are taken using the interference filter ($\lambda = 602$ nm) when β angle is 37° (d) and 75° (f). Polarizer is perpendicular to the rubbing direction. LC layer thicknesses are 6.5 μm.

Structure deformations are observed in the LC cell with $d = 6.5\,\mu$m and confinement ratio $d/p = 0.44$. In this case, the defects are observed in the form of elongated loops (Fig. 5a) or lines originating and ending at the cell edges (interfaces LC-air and LC-glue) or the surface defects. Therefore, the defects number near the edges of LC cell is more than in the central area. They are well observed independently of the polarization of incident light when the LC cell is placed between crossed polarizers. When observed the LC cell without analyzer the lines are clearly visible when the polarizer is parallel to the rubbing direction and the lines are almost invisible in the case of perpendicular polarization of incident light to the rubbing direction. The orientation of loops and their relative position can be different. At the same time, there is the twisted director structure between loops and the optical texture has the darkest state ($\lambda = 602$ nm) at $\beta \cong -40°$ (Fig. 5b).

At the wavelength of incident light λ is 602 nm the darkest state of optical texture, observed at $\beta \cong -40°$, corresponds to the azimuthal angle of director rotation $\varphi_d \cong 140°$. A couple of extinction bands near one of the loop line can be observed (Fig. 5b) by the analyzer rotation. As in the case of nematic described above the couple of extinction bands are gathered to the defect under the analyzer rotation. These lines are merged when the analyzer is almost parallel to the considered segment of the loop. Under further analyzer rotation the similar couple of extinction lines appears near the opposite segment of the loop and the distance between these lines depends on the β angle (Fig. 5b). Such orientation of extinction lines indicates that the director is oriented parallel to the line of loop defect on

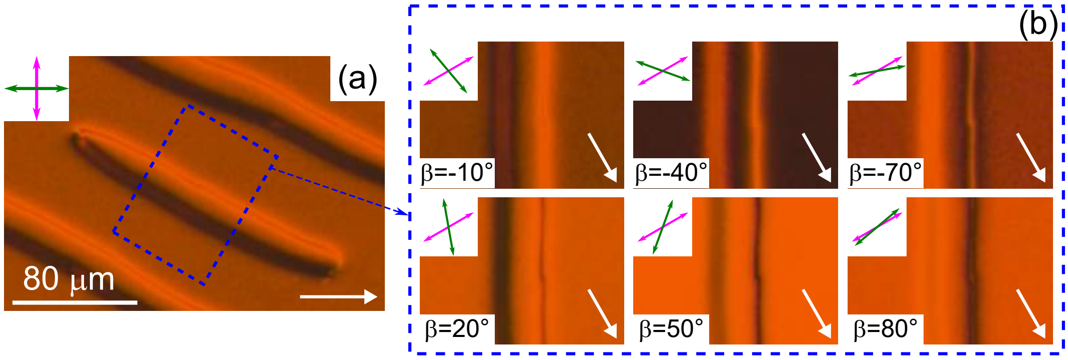

Figure 5. POM photos of cholesteric layer with confinement ratio $d/p = 0.44$ are taken using the interference filter ($\lambda = 602\,\text{nm}$). The angle β between analyzer and rubbing direction of PVA film is $0°$ (a). The magnified area of loop at different β angles (b). Polarizer is perpendicular to the rubbing direction. LC layer thickness is $6.5\,\mu$m.

the top substrate and $\pm\pi$ azimuthal rotation angle of director occurs between two opposite segments of the loop. Thus, the director turns by the various azimuthal angle near the defect and it is parallel to the substrate (tilt angle $\theta_d = 0°$) on the defect line itself. For example, the angle between the loop line and rubbing direction is approximately 30° (Fig. 5a). Consequently, the rotation angle φ_d is about 210° on the one loop segment and 30° on the opposite one.

The orientation with different angle of director rotation was simulated by the FDTD method (Fig. 6). The calculation was performed based on the spatial distribution of director in the cholesteric layer determined by the elastic energy minimization as in case of nematic. The section of defect loop by the plane perpendicular to the defect lines and oriented at 30° to the rubbing direction is shown in Fig. 6a. POM images of cholesteric layer with $d/p = 0.44$ for different β angles between analyzer and rubbing direction were calculated (Fig. 6b). It was revealed that the darkest state of optical texture corresponds to the $\beta = -40°$ far away from the defect. At the same time, the brightest optical texture is observed at $\beta = 50°$. The defect line corresponding to the smaller twist angle becomes dark when the analyzer is parallel to this line, i.e. it is parallel to the director on the top substrate. At that, the second defect line becomes dark when the angle between analyzer and wall is approximately 10°. It is explained by the fact that the effective refractive index near the walls has the larger value than that one far away from them. In this case the wavelength of incident light $\lambda = 602\,\text{nm}$ does not satisfy the Gooch-Terry minimum condition at large azimuthal twist of the director. As a consequence, the defect line with a large twist angle has the darkest state when the analyzer is not parallel to the director on the top substrate but this line is appreciably brighter than other sample areas at the minimum intensity condition of transmitted light. Spatial distribution of director on the substrate with conical boundary conditions is shown in Fig. 6c. Calculated data are in a good agreement with experimental results.

3.3. Periodic structure

Quasi-periodic structure of defects is formed in the LC cell with $d = 6.5\,\mu$m and confinement ratio $d/p = 0.44$ at the area close to the cell edge (Fig. 7a). The azimuthal angle of director rotation φ_d on the defect lines differs by π ($-\pi$) and between them φ_d has intermediate values (see Suppl. Fig.2). Similar periodic structure is observed through the whole cell area with $d/p = 0.60$ and in the samples with larger values of confinement ratio (Fig. 7b-d). The period of observed structure is about $2p$. The periodic structure was formed at similar values of confinement ratios d/p in the LC cells with tangential-weak conical boundary conditions [30], but the period was close to the cholesteric pitch. The disturbance of periodicity of two types can be observed in the samples (Fig. 7e). In the first case, the additional couple of defect lines appears leading to the local increasing of period near the region of line bending. In this area one defect line with larger azimuthal twist angle is smoothly transformed

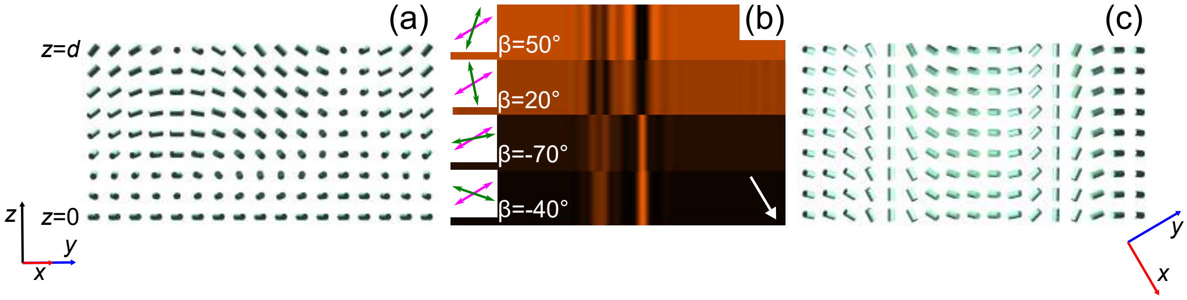

Figure 6. Calculated director configuration in the section perpendicular to the cell substrates and lines of defect (a). Simulated POM image of the area with couple of defects at different values of β angle between the analyzer and rubbing direction (b). The director orientation near the defect on the substrate covered with PiBMA (c). Polarizer is perpendicular to the rubbing direction. LC layer thickness is 6.5 μm and confinement ratio is $d/p = 0.44$.

into the defect line with a smaller φ_d angle. In the second case, some defect lines are formed and their orientation differs from the majority of defect lines. For example, some defect lines are oriented vertically in Fig. 7c. The periodic defect lines have 180° turn near these lines and do not intersect them. This way the defect line with larger azimuthal angle of director rotation is modified into line with smaller φ_d angle and vice versa.

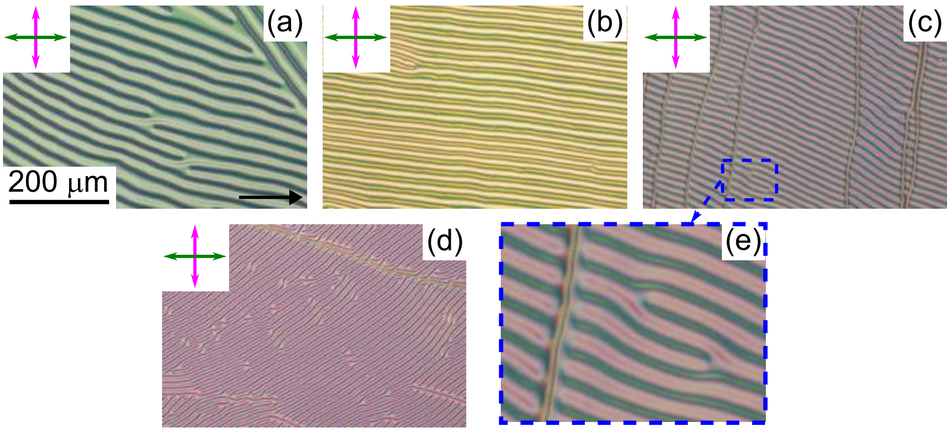

Figure 7. POM photos of cholesteric layer with confinement ratios d/p: 0.44 (a), 0.60 (b), 0.78 (c) and 0.88 (d). The magnified area with two types of defects of periodic structure at $d/p = 0.78$ (e). LC layer thicknesses are 6.5 μm.

It should be noted that the formation of defects and their periodic structure depends not only on the confinement ratio d/p but also on the value of cholesteric pitch (the thickness of LC layer). For example, the periodic structure is formed in the LC cell with $d/p = 0.60$ at $d = 6.5\,\mu$m ($p = 10.5\,\mu$m). But the twisted structure similar to the structure observed in LC cell with $d = 6.5\,\mu$m and $d/p = 0.44$ (Fig. 5, Fig. 7a) is formed in the sample with LC layer thickness $d = 13\,\mu$m ($p = 21\,\mu$m). The twisted structure with 185° azimuthal angle of director rotation containing a small number of defects is formed in the LC cell at $d = 21\,\mu$m ($p = 37\,\mu$m).

4. Conclusions

The orientational structures of nematic and cholesteric LC with the tangential-conical boundary conditions have been investigated. The cells with various LC layer thickness d and confinement ratio d/p have been considered. The domain structure is formed in the nematic LC cells containing the areas of positive and negative tilt angle of director at the substrate with conical boundary conditions. The domains are divided by the walls where the tilt angle of director is 0° at both substrates. The monodomain twisted structure without defects is formed in the cholesteric LC cell with $d = 6.5\,\mu$m and $d/p = 0.28$. At that, the azimuthal angle of director rotation is $\varphi_d = 75^\circ$ at the substrate with conical boundary conditions. Increase of the confinement ratio d/p up to 0.44 leads to the appearance of defects of elongated loop form. These topological defects are characterized by the difference of azimuthal angle of director rotation by $\pm\pi$ at the opposite segments of loop and 0° tilt angle of director at the defect. The periodic structure with a period close to the double cholesteric pitch is formed at $d/p \geq 0.60$ and more. The threshold value of d/p to form the periodic structure is relatively small. At the same time, this confinement ratio depends on the LC layer thickness (cholesteric pitch) in contrast to normal boundary conditions [16–18]. It is probably caused by the formation of two-dimensional defects in the system as well as the features of asymmetric boundary conditions in the cell.

Supplementary Materials: Figure S1, Figure S2.

Author Contributions: M.N.K. initiated this study; V.S.S. and M.N.K. performed the experiments and analysed the optical patterns, R.G.B. and I.V.T. performed a simulation of the orientation structures and optical texture, V.Y.Z. supervised the study. All authors wrote and reviewed the manuscript.

Funding: This work was supported by the Russian Science Foundation (No. 18-72-10036)

Conflicts of Interest: The authors declare no conflict of interest.

1. Oswald, P.; Pieranski, P. *Nematic and cholesteric liquid crystals: concepts and physical properties illustrated by experiments*; The liquid crystals book series, Taylor & Francis: Boca Raton, 2005.
2. Kim, J.H.; Huh, J.W.; Oh, S.W.; Ji, S.M.; Jo, Y.S.; Yu, B.H.; Yoon, T.H. Bistable switching between homeotropic and focal-conic states in an ion-doped chiral nematic liquid crystal cell. *Optics Express* **2017**, *25*, 29180–29188. doi:10.1364/OE.25.029180.
3. Hsiao, Y.C.; Tang, C.Y.; Lee, W. Fast-switching bistable cholesteric intensity modulator. *Optics Express* **2011**, *19*, 9744–9749. doi:10.1364/OE.19.009744.
4. Il'chishin, I.P.; Tikhonov, E.A.; Tishchenko, V.G.; Shpak, M.T. Generation of tunable radiation by impurity cholesteric liquid crystals. *JETP Letters* **1981**, *32*, 24–27.
5. Kopp, V.I.; Fan, B.; Vithana, H.K.M.; Genack, A.Z. Low-threshold lasing at the edge of a photonic stop band in cholesteric liquid crystals. *Optics Letters* **1998**, *23*, 1707–1709. doi:10.1364/OL.23.001707.
6. Subacius, D.; Bos, P.J.; Lavrentovich, O.D. Switchable diffractive cholesteric gratings. *Applied Physics Letters* **1997**, *71*, 1350–1352. doi:10.1063/1.119890.
7. Subacius, D.; Shiyanovskii, S.V.; Bos, P.; Lavrentovich, O.D. Cholesteric gratings with field-controlled period. *Applied Physics Letters* **1997**, *71*, 3323–3325. doi:10.1063/1.120325.
8. Senyuk, B.I.; Smalyukh, I.I.; Lavrentovich, O.D. Switchable two-dimensional gratings based on field-induced layer undulations in cholesteric liquid crystals. *Optics Letters* **2005**, *30*, 349. doi:10.1364/OL.30.000349.
9. Ryabchun, A.; Bobrovsky, A.; Stumpe, J.; Shibaev, V. Rotatable Diffraction Gratings Based on Cholesteric Liquid Crystals with Phototunable Helix Pitch. *Advanced Optical Materials* **2015**, *3*, 1273–1279. doi:10.1002/adom.201500159.
10. Lin, C.H.; Chiang, R.H.; Liu, S.H.; Kuo, C.T.; Huang, C.Y. Rotatable diffractive gratings based on hybrid-aligned cholesteric liquid crystals. *Optics Express* **2012**, *20*, 26837. doi:10.1364/OE.20.026837.
11. Liu, C.K.; Chiu, C.Y.; Morris, S.M.; Tsai, M.C.; Chen, C.C.; Cheng, K.T. Optically Controllable Linear-Polarization Rotator Using Chiral-Azobenzene-Doped Liquid Crystals. *Materials* **2017**, *10*, 1299. doi:10.3390/ma10111299.
12. Varney, M.C.M.; Zhang, Q.; Senyuk, B.; Smalyukh, I.I. Self-assembly of colloidal particles in deformation landscapes of electrically driven layer undulations in cholesteric liquid crystals. *Physical Review E* **2016**, *94*. doi:10.1103/PhysRevE.94.042709.
13. Dierking, I. *Textures of liquid crystals*; Wiley-VCH: Weinheim, 2003. OCLC: ocm51862996.
14. Ma, L.L.; Li, S.S.; Li, W.S.; Ji, W.; Luo, B.; Zheng, Z.G.; Cai, Z.P.; Chigrinov, V.; Lu, Y.Q.; Hu, W.; Chen, L.J. Rationally Designed Dynamic Superstructures Enabled by Photoaligning Cholesteric Liquid Crystals. *Advanced Optical Materials* **2015**, *3*, 1691–1696. doi:10.1002/adom.201500403.

15. Zheng, Z.g.; Li, Y.; Bisoyi, H.K.; Wang, L.; Bunning, T.J.; Li, Q. Three-dimensional control of the helical axis of a chiral nematic liquid crystal by light. *Nature* **2016**, *531*, 352–356. doi:10.1038/nature17141.
16. B. Ya. Zel'dovich.; Tabiryan, N.V. Freedericksz transition in cholesteric liquid crystals without external fields. *JETP Letters* **1981**, *34*, 406–408.
17. Cladis, P.E.; Kléman, M. The Cholesteric Domain Texture. *Molecular Crystals and Liquid Crystals* **1972**, *16*, 1–20. doi:10.1080/15421407208083575.
18. Goossens, W.J.A. The influence of homeotropic and planar boundary conditions on the field induced cholesteric-nematic transition. *Journal de Physique* **1982**, *43*, 1469–1474. doi:10.1051/jphys:0198200430100146900.
19. Oswald, P.; Baudry, J.; Pirkl, S. Static and dynamic properties of cholesteric fingers in electric field. *Physics Reports* **2000**, *337*, 67–96. doi:10.1016/S0370-1573(00)00056-9.
20. Varanytsia, A.; Posnjak, G.; Mur, U.; Joshi, V.; Darrah, K.; Muševič, I.; Čopar, S.; Chien, L.C. Topology-commanded optical properties of bistable electric-field-induced torons in cholesteric bubble domains. *Scientific Reports* **2017**, *7*. doi:10.1038/s41598-017-16241-4.
21. Ackerman, P.J.; Qi, Z.; Smalyukh, I.I. Optical generation of crystalline, quasicrystalline, and arbitrary arrays of torons in confined cholesteric liquid crystals for patterning of optical vortices in laser beams. *Physical Review E* **2012**, *86*, 021703. doi:10.1103/PhysRevE.86.021703.
22. Ackerman, P.J.; Trivedi, R.P.; Senyuk, B.; van de Lagemaat, J.; Smalyukh, I.I. Two-dimensional skyrmions and other solitonic structures in confinement-frustrated chiral nematics. *Physical Review E* **2014**, *90*, 012505. doi:10.1103/PhysRevE.90.012505.
23. Kim, Y.H.; Gim, M.J.; Jung, H.T.; Yoon, D.K. Periodic arrays of liquid crystalline torons in microchannels. *RSC Advances* **2015**, *5*, 19279–19283. doi:10.1039/C4RA16883F.
24. Andrienko, D. Introduction to liquid crystals. *Journal of Molecular Liquids* **2018**, *267*, 520–541. doi:10.1016/j.molliq.2018.01.175.
25. Belyaev, S.V.; Rumyantsev, V.G.; Belyaev, V.V. Optical and electro-optical properties of confocal cholesteric textures. *JETP* **1977**, *46*, 337–340.
26. Belyaev, S.V.; Blinov, L.M. Instability of planar texture of a cholesteric liquid crystal in an electric field. *JETP* **1976**, *43*, 96–99.
27. Nose, T.; Miyanishi, T.; Aizawa, Y.; Ito, R.; Honma, M. Rotational Behavior of Stripe Domains Appearing in Hybrid Aligned Chiral Nematic Liquid Crystal Cells. *Japanese Journal of Applied Physics* **2010**, *49*, 051701. doi:10.1143/JJAP.49.051701.
28. Kumar, T.A.; Le, K.V.; Aya, S.; Kang, S.; Araoka, F.; Ishikawa, K.; Dhara, S.; Takezoe, H. Anchoring transition in a nematic liquid crystal doped with chiral agents. *Phase Transitions* **2012**, *85*, 888–899. doi:10.1080/01411594.2012.692092.
29. Tran, L.; Lavrentovich, M.O.; Durey, G.; Darmon, A.; Haase, M.F.; Li, N.; Lee, D.; Stebe, K.J.; Kamien, R.D.; Lopez-Leon, T. Change in Stripes for Cholesteric Shells via Anchoring in Moderation. *Physical Review X* **2017**, *7*, 041029. doi:10.1103/PhysRevX.7.041029.
30. Zola, R.S.; Evangelista, L.R.; Yang, Y.C.; Yang, D.K. Surface Induced Phase Separation and Pattern Formation at the Isotropic Interface in Chiral Nematic Liquid Crystals. *Physical Review Letters* **2013**, *110*, 057801. doi:10.1103/PhysRevLett.110.057801.
31. Timofeev, I.V.; Lin, Y.T.; Gunyakov, V.A.; Myslivets, S.A.; Arkhipkin, V.G.; Vetrov, S.Y.; Lee, W.; Zyryanov, V.Y. Voltage-induced defect mode coupling in a one-dimensional photonic crystal with a twisted-nematic defect layer. *Phys. Rev. E* **2012**, *85*, 011705. doi:10.1103/PhysRevE.85.011705.
32. Krakhalev, M.N.; Prishchepa, O.O.; Sutormin, V.S.; Zyryanov, V.Y. Director configurations in nematic droplets with tilted surface anchoring. *Liquid Crystals* **2017**, *44*, 355–363. doi:10.1080/02678292.2016.1205225.
33. Rudyak, V.Y.; Krakhalev, M.N.; Prishchepa, O.O.; Sutormin, V.S.; Emelyanenko, A.V.; Zyryanov, V.Y. Orientational structures in nematic droplets with conical boundary conditions. *JETP Letters* **2017**, *106*, 384–389. doi:10.1134/S0021364017180102.
34. Rudyak, V.Y.; Krakhalev, M.N.; Sutormin, V.S.; Prishchepa, O.O.; Zyryanov, V.Y.; Liu, J.H.; Emelyanenko, A.V.; Khokhlov, A.R. Electrically induced structure transition in nematic liquid crystal droplets with conical boundary conditions. *Physical Review E* **2017**, *96*, 052701. doi:10.1103/PhysRevE.96.052701.

35. Vilanove, R.; Guyon, E.; Mitescu, C.; Pieranski, P. Mesure de la conductivité thermique et détermination de l'orientation des molécules a l'interface nématique isotrope de MBBA. *Journal de Physique* **1974**, *35*, 153–162. doi:10.1051/jphys:01974003502015300.
36. Gilli, J.; Morabito, M.; Frisch, T. Ising-Bloch transition in a nematic liquid crystal. *Journal de Physique II* **1994**, *4*, 319–331. doi:10.1051/jp2:1994131.
37. Ryschenkow, G.; Kleman, M. Surface defects and structural transitions in very low anchoring energy nematic thin films. *The Journal of Chemical Physics* **1976**, *64*, 404–412. doi:10.1063/1.431934.
38. Gooch, C.H.; Tarry, H.A. The optical properties of twisted nematic liquid crystal structures with twist angles ≤ 90 degrees. *Journal of Physics D: Applied Physics* **1975**, *8*, 1575–1584. doi:10.1088/0022-3727/8/13/020.
39. Yeh, P.; Gu, C. *Optics of liquid crystal displays*; Wiley series in pure and applied optics, Wiley: New York, 1999.